European Journal of Soil Science

European Journal of Soil Science, September 2016, **67**, 583–596 doi: 10.1111/ejss.12363

Incipient ferralization and weathering indices along a soil chronosequence in Taiwan

S.-H. Jien[a], I. Baillie[b], W.-S. Huang[c], Y.-Y. Chen[d] & C.-Y. Chiu[e]

[a]*Department of Soil and Water Conservation, National Pingtung University of Science and Technology, Pingtung, 912-01, Taiwan,* [b]*National Soil Resources Institute, Cranfield University, Cranfield, MK43 0AL, UK,* [c]*Department of Geography, National Changhua University of Education, Changhua, 500, Taiwan,* [d]*Institute of Physics, Academia Sinica, Taipei, 115-29, Taiwan, and* [e]*Biodiversity Research Center, Academia Sinica, Taipei, 115-29, Taiwan*

Summary

The low hilly topography of Green Island, a volcanic island off southeastern Taiwan, includes an altitudinal sequence of sub-horizontal benches. We examined eight profiles along this sequence, ranging from pale brown loamy coral sand on the lowest bench that fringes the coast at an elevation of about 10 m to deep, intensely red and acid clay on the highest bench at about 240 m. Chemical analyses, differential Fe extractions, thin sections, X-ray diffraction of the clay minerals and indices of pedochemical weathering and strain indicated that soil development progressed by weathering of primary and secondary phyllosilicates through argilluviation in the intermediate stages to the generation of increasing quantities of free Fe. The Fe accumulates as free sesquioxides, which crystallize with age. Taxonomically the soil types progress from sandy coral Arenosol, through Eutric Cambisol, Hypereutric Lixisol and Acrisol to incipient Ferralsol (Udipsamment → Eutrudept → Udalf → Udultisol → Udox in Soil Taxonomy). The profiles are interpreted as a chronosequence, although this is complicated by minor and upwardly diminishing contributions of reef coral to the mainly igneous parent materials. There are also variations in the andesitic-basaltic bedrock, and minor aeolian inputs in the higher and older soil types. Regional eustatic sea-level correlations, ^{14}C dating of carbonates on the two lowest benches and estimates of local tectonic uplift indicate that the incipient Ferralsols on the upper bench might date from about 150 ka. The transition through argilluvial Acrisols to incipient sesquioxide-dominated Ferralsols appears, therefore, to develop within 100–200 ka on Green Island, which is faster than usual.

Highlights

- Green Island (Taiwan) has been volcanically dormant but tectonically active for 2 million years.
- The island has a toposequence of bevelled surfaces with relatively uniform andesitic regoliths.
- The soils of the surfaces form a chronosequence from Arenosols through Acrisols to incipient Ferralsols.
- The transition from argilluvial to ferralitic pedogenesis, at 100–200 ka, is relatively rapid.

Introduction

Acrisols (IUSS Working Group WRB, 2015) and Ultisols, their approximate equivalents in Soil Taxonomy (Soil Survey Staff, 2014), are extensive in many stable tropical landscapes, and appear to be the culmination of tropical pedogenesis on argillaceous sedimentary parent materials (Baillie, 1996). They are also extensive in warm extra-tropical areas with summer rainfall, such as the southeastern USA and southern China, where they are perceived to be the final stage of soil development, as indicated by their name in Soil Taxonomy. They are deep and well weathered and are characterized by increasing clay contents and reddening with depth. Their subsoils have a moderately firm blocky structure with pronounced clay skins and clay translocation appears to be an important process. Kandites are the main clay minerals, but there are sufficient contents of moderately expansible 2:1 phyllosilicates to generate a blocky structure and enough free sesquioxides to give bright colours. They are leached, acid and of low exchangeable base status.

In some humid tropical landscapes on crystalline and feldspathic sandstone parent materials, texturally segregated Acrisols predominate only on topographic 'shoulders' and other active slope elements. The soil on more stable plateau and interfluve

Correspondence: C.-Y. Chiu. E-mail: bochiu@sinica.edu.tw

Received 4 May 2015; revised version accepted 5 May 2016

sites is deep, texturally homogenous, intensely reddened, and rich in sesquioxides and friable Ferralsol (Oxisol in Soil Taxonomy) (Beinroth *et al.,* 1974). There are site-specific variations in this pattern of Acrisols on slopes and Ferralsols on plateaux, but it is sufficiently widespread to indicate that Acrisols are not the end stage of pedogenesis in many non-argillaceous regoliths in the humid tropics. It appears that there is a late transition from predominantly phyllosilicate argilluvial to texturally homogenizing and sesquioxide-accumulating ferralitic pedogenesis. In addition to reddening the soil, the accumulating Fe sesquioxides stabilize porous biogenic structures to give compound peds of blocks that break to a friable micro-crumb structure. The sesquioxides become increasingly crystallized with age and might segregate spatially to form plinthite and eventually ferricrete in soil with variable moisture regimes. An alternative interpretation of the textural differentiation and other features of the Acrisols is that they result from the downward movement of weathering fronts rather than from argilluviation, and that the transition to ferralization is a late stage in this progression (Legros, 2012).

Because argilluviation and ferralization are too slow to be observed and quantified directly within human time-scales, their development is often inferred from chronosequences, in which ordered spatial sequences are interpreted as temporal transects. Pedological chronosequences are identified and characterized by the soil differences that develop in lithologically similar regoliths of increasing age. The age differences might result from successive phases of glacial, aeolian or volcanic deposition, or from episodic depression of local erosional base levels caused by tectonic uplift or sea-level changes or both. Alluvial terraces are favoured for pedochronological studies because their stepped sequences provide apparently clear age progressions. Soil chronosequences are also present in some anthropogenic regoliths, but their time-scales are too short to elucidate slow pedogenic processes.

A general problem with soil chronosequences is the attribution of observed differences to time and increased soil maturity, on the assumption that other factors of pedogenesis remain relatively constant. Some soil chronosequences go back to the early Pleistocene and beyond, and their older members have been exposed to considerable fluctuations in climate, moisture status and biotic interactions (Vitousek, 2004). Geomorphological turbulence during the Pleistocene means that many older regoliths have been overlaid, truncated and mixed since emplacement. Uncritical application of the simple chronological form of Jenny's (1980) soil formation function,

$$\text{Soil} = \text{function of time (with climate, organisms, relief and parent material as constants)},$$

is rarely possible in long sequences. Nevertheless, it appears to be more or less valid in studies of low and fairly recent terraces, such as in the sequences of coral soil on uplifted marine benches on the southeast coast of Taiwan (Huang *et al.,* 2010) and of alluvial soil on river terraces inland (Tsai *et al.*, 2006).

In this study we examined the soil on an altitudinal sequence of bevelled surfaces on Green Island off the southeastern coast of Taiwan. The soil changes from coral sand on the lowest terrace to ferralitic red clays derived from andesite on the upper surfaces. These soils are interesting because few terrace chronosequences are long enough to include the transition from argilluvial to ferralitic soil. Our aim is to quantify the apparently rapid rates of weathering and pedogenesis along this chronosequence.

Materials and methods

Study site

Green Island, also known as Ludao (22°40′35.5″N; 121°27′59″E), is 33 km off the southeastern coast of Taiwan (Figure 1 inset). It consists of irregular low hills, with an altitudinal series of extensive but discontinuous sub-horizontal benches (Table 1) that result in compound slopes (Figure 1). Chen & Liu (1992) identified the benches as marine terraces and suggested that they can be attributed to a combination of tectonic movement and changes in sea level within a single transgression–regression cycle.

The island is on the Yangstse section of the Eurasian continental plate, close to the tri-junction with the northern end of the Luzon arc and the subducting margin of the oceanic Philippine Sea plate. It is volcanic and consists mainly of Miocene and Pliocene pyroclastic deposits and lava flows. Hornblende-pyroxene, olivine-pyroxene, hornblende and biotitic andesites predominate, but there are also some tholeitic basalts. There has been no volcanic activity for about 2 Ma, but spasmodic uplift has continued during the Quaternary and the island is still moderately seismically active (Ho, 1988). Reefs formed along the coast during the Quaternary, and local uplift has combined with changes in sea level to give distinct coral benches at 2–15 and 20–50 m above current sea level (Figure 1). The 2–15-m bench consists of massive pocketed coral covered by variable depths of pale coralline sand. There are also visible fragments of coral in the soil on the intermediate benches at 50–70 and 85–95 m. Coral has also been reported in progressively diminishing quantities on the 100, 170, 190 and 240-m benches (Chen & Liu, 1992), but we saw none on these surfaces in the course of our study, and the profiles examined on them appear to be almost wholly derived from igneous residua and colluvia.

The climate is tropical oceanic with a mean annual air temperature of 23.5°C, and monthly means range from 20 to 30°C. The mean annual rainfall is about 2500 mm, but appears to be less on west-facing slopes. The rainfall is seasonally bimodal, with peaks in the summer monsoon and again in the July to November typhoon season. The natural vegetation for the whole island was originally subtropical broadleaf forest, and the two highest benches (at 190 and 240 m) still have some forest cover. The island has a long history of settlement and the forest was mostly cleared, although cultivation has decreased recently. Much of the former agricultural land is now anthropogenic grassland with scattered screw pine (*Pandanus tectorius* Parkinson) or has been invaded by low secondary forest dominated by *Leucaena leucocephala* (Lam.) de Wit. The lower benches are covered by screw pine scrub.

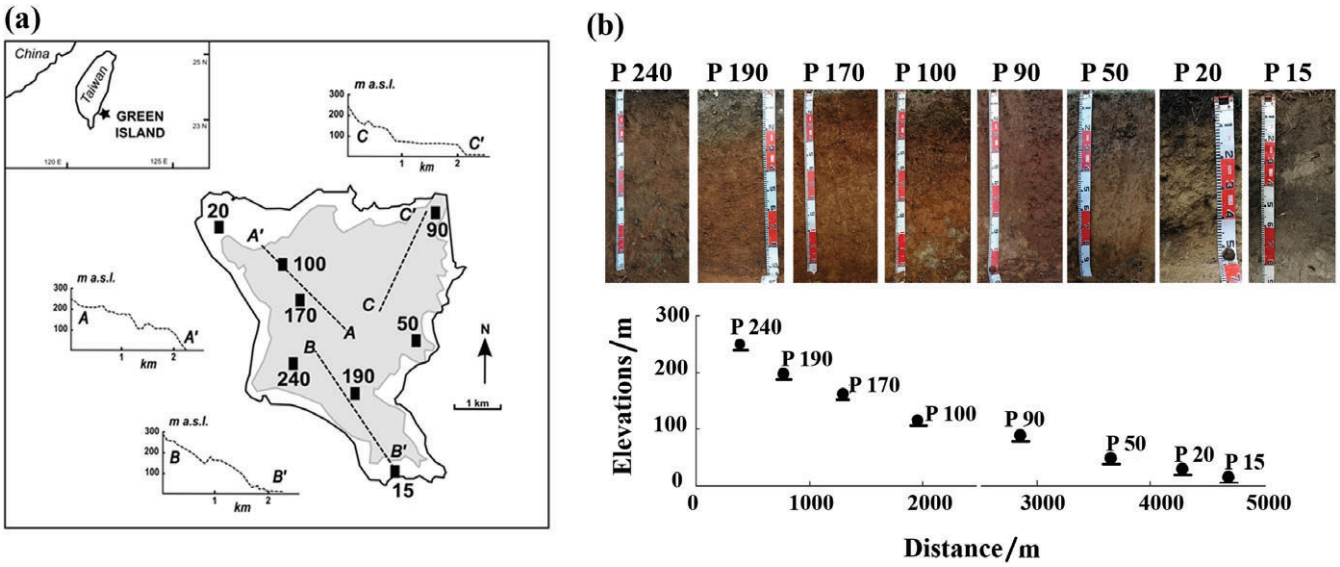

Figure 1 Location of (a) topographic transects and (b) profiles, Green Island, Taiwan. Shaded, andesite bedrock; Unshaded, Late Quaternary reef coral.

Table 1 Study sites

Profile	Bench elevation / m a.s.l.	Vegetation
15	2–5	Scrub of Screw Pine (*Pandanus tectorius* Parkinson)
20	20–50	Scrub of *Pandanus tectorius*
50	50–70	Grassland
90	85–95	*Pandanus tectorius* Parkinson scrub and grassland
100	100–150	Grassland
170	170	Broad-leaved forest with *Pandanus tectorius* Parkinson
190	190	Broad-leaved forest
240	240	Broad-leaved forest

Soil description and analysis

We described and sampled eight soil profiles that are numbered 15, 20, 50, 90, 100, 170, 190 and 240 according to bench elevations. We collected undisturbed blocks of soil in 8 cm × 5 cm Kubiena boxes and also disturbed samples from 27 soil horizons (Table 1 and Figure 1). The disturbed samples were air-dried, ground, sieved to 2 mm and analysed by conventional methods (Klute, 1986): particle-size distribution was determined by the pipette method, soil pH was determined electrometrically in 1:2.5 soil:water suspension, soil organic carbon (SOC) content was measured with a Fisons NA1500 elemental analyser (ThermoQuest Italia, Milan, Italy), cation exchange capacity (CEC) was measured and exchangeable bases were extracted with ammonium acetate buffered at pH 7, the elements were assayed by atomic absorption spectrometry (AAS) and CEC:clay was estimated with an adjustment for the contribution from organic matter (Van Reeuwijk, 1993). The total contents of all elements were determined by X-ray fluorescence (XRF) (Rigaku ZSX Mini II XRF Analyzer, Tokyo, Japan), with calibration against the NIST-2709 standard reference material (National Institute of Standards and Technology, Gaithersburg, MD, USA). Pedochemical weathering indices and mass-balance changes (Egli & Fitze, 2000) were estimated from the XRF data. Free Fe and Al (Fe_d and Al_d) were extracted with dithionite-citrate-bicarbonate (DCB) and amorphous Fe and Al (Fe_o and Al_o) with ammonium oxalate at pH 3. The Fe and Al contents of the extracts were assayed by AAS. Contents of crystalline Fe and Al were estimated as $Fe_d - Fe_o$ and $Al_d - Al_o$.

We used the data to derive the aluminium oxide index, also known as the chemical index of alteration (CIA):

$$CIA = Al_2O_3/\left(Al_2O_3 + CaO + Na_2O + K_2O\right) \times 100,$$

and the base depletion index (BDI):

$$BDI = \left(CaO + MgO + Na_2O + K_2O\right) / \left(Fe_2O_3 + Al_2O_3 + TiO_2\right),$$

and two desilication indices (DSI):

$$DSI = SiO_2/Al_2O_3 \text{ and } SiO_2/\left(Fe_2O_3 + Al_2O_3\right).$$

The iron sesquioxides were characterized by the $(Fe_d - Fe_o)/Fe_t$ ratio of crystalline sesquioxides to total Fe, and the Fe_o/Fe_d activity ratio of amorphous to free Fe sesquioxides (Blume & Schwertmann, 1968).

Pedogenic strain (ε) summarizes the changes in mass proportions of elements in the solum relative to the parent material (Brimhall & Dietrich, 1987; Egli & Fitze, 2000; Egli *et al.*, 2008). It indicates whether increasing proportions of a component result from residual accumulation as other components are depleted or from active importation (Egli *et al.*, 2008). Mass-balance calculations and the

calculation of time-averaged weathering rates of soil profiles or soil horizons define strain on volume change:

$$\varepsilon_{i,\mathrm{w}} = \frac{\Delta z_{\mathrm{w}}}{\Delta z} - 1, \quad (1)$$

where i is selected element, Δz is the columnar height of a representative elementary volume of rock and Δz_{w} is the weathered equivalent height 'w'. The curves derived were determined by the results and were not constrained to pass through the origin.

After air-drying the Kubiena tins, $5\,\mathrm{cm} \times 8\,\mathrm{cm} \times 30\,\mu\mathrm{m}$ thin sections were prepared by Spectrum Petrographics, Inc. (Winston, Oregon, USA) and described with a polarizing microscope (AFX-II, Nikon Precision Instruments, Belmont, CA, USA) using the terminology of Stoops (2003). Clay mineralogy was examined in oriented clay samples with an X-ray diffractometer (XRD) (Rigaku D/max-2200/PC type, Tokyo, Japan; Ni-filtered Cu-Kα radiation generated at 30 kV and 10 mA). The XRD patterns were recorded at a scanning speed of 0.5° (2θ) minute^{-1} from 3° to 60° (2θ). The identification and semi-quantitative estimates of the clay minerals were based on differences in the reflection patterns from samples that were variously pretreated by K-saturation, Mg-saturation, glycolation, heating and air-drying (Brindley & Brown, 1980).

Principal component analysis

To interpret the relations between the numerous morphological and laboratory variables and to clarify underlying pedogenic trends, we examined the data by a principal component analysis (PCA). We used the correlation matrix because the variables were measured on different scales. Of the particle size variables, we retained clay and silt and omitted sand in order to avoid linear dependence. For the same reason we deleted cation exchange capacity so that we could retain the individual exchangeable cations and also base saturation, which is a criterion in the international soil classification systems. Our discussion focuses on the first two components; they accounted for almost two-thirds of the total variance. All analyses were performed with IBM SPSS Statistics, Version 22 (Somers, NY, USA).

Results

Soil morphology

Colours of the subsoil matrix become redder with elevation; they range from pale and greyish brown in profile 15, through reddish brown at intermediate levels, to intensely red on the higher benches (Table 2). The texture of the subsoil of profile 15 is loamy sand and that of profile 20 is silty loam, but the soils on the higher benches are all clays (Tables 2, 3). Angular blocky structures with more or less continuous clay coatings predominate in the clay subsoil; the structural development increases from moderate to strong with increasing elevation. The bright red and slightly firm Bt horizon in profile 240 had a strong angular blocky structure, with a tendency to break down to crumbs. All of the samples of clay soil were sticky and plastic when wetted (Table 2). There were no free carbonates in profiles 240, 190, 170 and 100, but profile 90 had a weak reaction to HCl and profiles 50, 20 and 15 had moderate or strong reactions (Table 3).

The thin section of the coarse-textured C horizon in profile 15 had a grey soil matrix with sand fragments of coral, loose structure, and an equal double-spaced enaulic c/f-related distribution (Figure 2a), where c/f refers to coarse relative to fine. The thin section of the weakly structured Bw/BC horizons of profile 20 had a pale yellow matrix with a speckled b-fabric (birefringence fabric), which means that these horizons are characterized by randomly arranged, equidimensional or slightly prolate domains of oriented clay, smaller than the fabric units at the scale of observation, and a double-spaced porphyric c/f-related distribution, and infrequent argillans (Figure 2b). The Bt horizon of profile 100 had a moderate blocky structure, and its thin section showed a brown coloured crystalline b-fabric, with clear argillans (Figure 2c,d). The thin section of the Bt horizon in profile 240 was dark red in plane-polarized light and changed to black (isotropic) in cross-polarized light. It has a vughy microstructure (more or less equidimensional, irregular voids, smooth or rough, not usually interconnected to voids of comparable size) with an undifferentiated b-fabric and coarse to fine open porphyric c/f-related distribution (Figure 2e,f).

The granulometric analyses accord with the distribution of visible clay skins (Table 2) and the thin sections (Figure 2) with moderate or weak clay maxima (Table 3) that indicate apparently argilluvial subsoil on the intermediate benches, although some are too weak to meet the argillic criteria of the World Reference Base or Soil Taxonomy. There were no subsoil clay maxima or visible clay skins in profiles 20 and 15, and no clay maximum within the solum of profile 240. The underlying C horizons are all more sandy than the sola.

Soil chemical properties

The soil on the upper benches is acidic (pH < 5.5), but profiles 100, 20 and 15 have a pH near neutral (Table 3). The topsoil contents of SOC are moderate under forest or dense scrub, but small to moderate in anthropogenic grassland soil at intermediate levels. Cation exchange capacity (CEC) values ranged from 8 to 22 cmol(+) kg^{-1}. The soils of the profiles above 170 m were intensively leached with a base saturation (BS) < 35%, whereas it exceeded 50% in profile 100 and at lower elevations. The subsoil CEC/clay values, corrected for organic matter, increased with elevation, but were still mostly within or close to the definitions of ferralic or oxic horizons.

Total iron contents (Fe_t) were moderate to large (45–99 g kg^{-1}) in profile 240 and down to profile 50, but small (0–0.64 g kg^{-1}) in profiles 20 and 15. Contents of free iron (Fe_d) and aluminium (Al_d) were largest in the B horizons. They increase with elevation from small in profiles 15–50, through moderate in profiles 90–170 to large in profiles 190 and 240 (Table 4). Contents of amorphous and poorly crystalline sesquioxides are small throughout; Fe_o ranges from 1.35 to 9.72 g kg^{-1} and Al_o from 3.28 to 9.14 g kg^{-1}. The

Table 2 Soil macromorphology

Profile	Horizon	Depth / cm	Matrix colour	Texture[a]	Structure[b]	Consistence[c] (moist)	Root[d]	Clay skins[e]	Stone / %	Lower boundary[f]
15	A	0–25	10YR 3/1	LS	Structureless	ss&sp	3vf&f&m	–	–	gi
	C1	25–50	10YR 2/1	LS	Structureless	ns&np	3vf&f; 2m	–	10	cs
	C2	50–70	10YR 2/1	LS	Structureless	ns&np	3vf&f; 2m	–	10	cs
	C3	70–90	10YR 6/4	LS	Structureless	ns&np	2vf&f&m	–	25	–
20	A	0–10	2.5Y 2.5/1	SiL	2vf&f gr	ss&sp	3vf&f	–	–	cs
	Bw	10–25	2.5Y 4/3	SiL	2vf&f abk;	ss&sp	2vf&f	2dpf	30	gs
	BC	25–70	2.5Y 4/4	SiL	2vf&f abk;	ss&sp	2vf&f	–	50	d
	C	> 70	–	–	–	–	–		50	–
50	A	0–25	5YR 3/3	C	1vf&f abk; 2 vf&f gr	s&p	3vf&f	–	–	gs
	Bt	25–50	7.5YR 3/4	C	2vf&f abk	vs&vp	2vf&f	3dpf	–	cs
	2A	50–75	5YR 3/2	C	2vf&f abk;	s&p	1vf&f	2dpf	–	gs
	2Bt	75–100	5YR 3/4	C		vs&vp	1vf&f		–	d
	3C	100–130	7.5YR 5/6	CL	–	–	–	–	30	–
90	A	0–10	2.5YR 3/3	C	2vf&f abk	s&p	3vf&f	–	–	d
	AB	10–25	2.5YR4/4	C	2vf&f abk	s&p	3vf&f	3dpf	–	gs
	Bt1	25–48	2.5YR 4/5	C	2vf&f abk	vs&vp		3dpf	5	cs
	Bt2	48–75	2.5YR4/5	C	2vf&f abk	vs&vp	1vf&f	2dpf	5	ci
	2BC	75–100	5YR 4/6	C	2 vf,&m abk	s&p	–	–	50	–
100	A	0–18	7.5YR 3/3	C	2vf&f abk	s&p	3vf&f &m	–	–	d
	AB	18–35	7.5YR 3/4	C	3vf&f abk	vs&vp	3vf&f &m	–	–	gs
	Bt1	35–67	2.5YR 3/6	C	3 vf;f&m abk	vs&vp		3dpf	2	gs
	Bt2	67–92	2.5YR 4/7	C	3 vf;f&m abk	vs&vp	1vf&f	3dpf	5	d
	BC	> 92	5YR 4/6	SiC	2vf;f&m abk	s&p	–	–	60	–
170	A	0–24	2.5YR 3/3	C	2vf&f abk	s&p	3vf&f; 2m&1c	–	–	cs
	Bt1	24–50	2.5YR 4/6	C	3vf&f abk	vs&vp	3vf&f; 2m	3dpf	–	d
	Bt2	50–75	2.5YR 4/6	C	3f&m abk	vs&vp	2vf; f&m	3dpf	–	d
	Bt3	70–100	2.5YR 4/6	C	3f&m abk	vs&vp	2vf&f; 3m	3dpf	–	d
	Bt4	100–140	5YR 4/6	C	3f&m abk	vs&vp	2vf&f; 3m	3dpf	–	d
	C	> 200	7.5YR 5/4	SiCL	–	–	–	–	100	
190	A	0–20	2.5YR 3/3	C	2vf&f gr; 2vf&f abk	s&p	3vf;f&m	–	–	gw d
	2Bt1	20–45	2.5YR 3/6	C	2f&m abk	vs&vp	2vf&f	3dpf	–	d
	2Bt2	45–70	2.5YR 4/6	C	2f&m abk	vs&vp	2vf&f	3dpf	–	d
	2Bt3	70–100	2.5YR 4/6	C	2f&m abk	vs&vp	2vf&f	3dpf	–	–
240	A	0–15	5YR 3/2	C	2vf&f gr; 2vf&f abk	s&p	2m; 1c	– 3dpf	–	gw
	Bt1	15–40	2.5YR 3/6	C	2f&m abk	vs&vp	3vf&f; 2m	3dpf	–	d
	Bt2	40–60	2.5YR 4/6	C	2f&m abk	vs&vp	3vf&f; 2m	3dpf	–	cw
	BC	60–80	2.5YR 4/6	C	2vf&f abk	vs&vp	3vf&f; 2m	3dpf	10	gw

[a]LS, loamy sand; SiL, silt loam; C, clay; SiC, silty clay.
[b]1 = weak, 2 = moderate, vf = very fine, f = fine, m = medium, gr = granular, abk = angular blocky, sbk = subangular blocky.
[c]fm = firm, fri = friable, s = sticky, p = plastic, np = non–plastic, ss = slightly sticky, sp = slightly plastic, vs = very sticky, vp = very plastic.
[d]c = common, m = many, s = some, f = few, c = coarse, m = medium, f = fine, vf = very fine.
[e]1 = few, 2 = common, 3 = many, f = faint, d = distinct, pf = ped surface.
[f]a = abrupt, c = clear, s = smooth, g = gradual, d = diffuse, w = wavy, i = irregular, b = broken.
– : No gravels were found in the horizon.

crystallinity of the free Fe sesquioxides ($(Fe_d - Fe_o) / Fe_t$) increases with elevation from < 0.2 in profile 15 to > 0.8 in profile 240 (Table 4 and Figure 3). Iron activity decreases exponentially with elevation (Figure 3):

$$Fe_o/Fe_d = 1.07 \cdot a^{-3.64\,((Fe_d - Fe_o)/Fe_t)},$$

where a is altitude (m a.s.l.). The decrease is more or less asymptotic at about 0.1 in the profiles above 100 m. Table 5 shows increases in Al_t and Al_d and decreases in Al_o/Al_d with elevation, but these are small and erratic, which accords with the moderate but variable XRD peaks for gibbsite.

The main contributors to overall strain are the accumulations of Fe and Al sesquioxides and the losses of basic cations and Si. The largest values of strain are in the topsoil of profile 240 (Table 6) and might be accentuated by organic matter content (Nieuwenhuyse & van Breemen, 1997). The depletion of basic cations appears to be

Table 3 Granulometry and chemical properties

Profile	Horizon	Sand/ %	Silt/ %	Clay/ %	pH	SOC[a]/ %	Exchangeable K / cmol(+) kg^{-1}	Na / cmol(+) kg^{-1}	Ca / cmol(+) kg^{-1}	Mg / cmol(+) kg^{-1}	CEC[b] / cmol(+) kg^{-1}	BS[c] / %	Reaction with 1 M HCl
15	A	81.4	9.82	8.75	8.05	6.88	0.12	0.78	81.2	1.17	1.0	100	++[d]
	C1	85.2	5.52	9.25	8.39	3.96	0.14	0.57	40.7	1.03	3.0	100	++
	C2	85.0	6.06	8.99	7.77	4.14	0.09	0.59	40.5	0.97	1.6	100	++
	C3	89.9	2.68	7.37	8.54	2.21	0.02	0.43	46.2	1.30	1.3	100	++
20	A	33.4	55.2	11.4	7.29	5.60	1.86	1.76	19.7	3.27	23.8	100	+
	Bw	41.1	44.6	14.3	6.79	0.79	1.20	2.48	4.64	0.82	13.2	69.0	+
	BC	37.6	47.4	15.0	6.84	0.19	0.42	3.25	4.61	0.53	11.1	79.0	–
	C	54.7	36.6	8.8	7.10	0.11	0.37	1.28	3.47	0.67	6.5	89.0	–
50	A	3.70	19.9	76.3	5.16	2.36	1.12	0.73	4.23	2.11	11.8	69.4	+
	Bt	4.20	19.6	76.2	5.00	1.61	0.72	1.21	2.19	2.11	10.5	59.3	+
	2A	3.80	29.4	66.8	5.28	2.56	0.24	0.69	2.33	1.31	9.1	50.2	+
	2Bt	1.30	22.3	76.4	5.07	1.57	0.21	0.79	1.75	1.28	9.0	44.3	–
	3C	26.1	41.9	32.0	4.61	0.23	0.80	6.21	2.02	1.53	12.5	84.5	–
90	A	4.50	23.3	72.2	5.04	3.28	0.75	1.48	4.12	3.23	13.8	79.3	+
	AB	4.93	20.0	75.1	5.28	2.50	0.68	1.25	3.59	3.09	11.3	86.5	+
	Bt1	5.20	20.1	74.7	5.18	1.73	0.67	1.29	3.99	3.03	11.8	85.0	–
	Bt2	9.40	22.1	68.5	5.28	1.30	0.60	1.45	2.88	3.05	14.2	65.1	–
	2BC	24.4	27.0	48.6	5.16	0.30	1.00	3.92	2.42	2.84	17.8	71.0	–
100	A	5.85	30.0	64.1	6.44	2.73	0.22	0.53	10.5	1.56	8.8	100	–
	AB	5.99	26.1	67.9	7.42	2.01	0.25	0.84	28.6	1.40	9.9	100	–
	Bt1	2.85	29.7	67.5	7.44	0.77	0.28	1.44	11.5	0.96	8.3	100	–
	Bt2	2.01	27.4	70.6	7.15	0.88	0.12	2.08	14.6	0.57	11.5	98.5	–
	BC	17.4	42.1	40.5	6.90	0.31	0.01	1.89	10.7	0.27	11.5	100	–
170	A	2.29	20.7	77.0	4.02	2.84	0.25	1.83	0.15	0.15	8.7	29.3	–
	Bt1	0.97	10.6	88.4	4.52	0.82	0.07	1.77	0.01	0.45	9.0	27.4	–
	Bt2	0.98	8.49	90.5	4.69	0.76	0.06	0.79	0.08	0.52	9.2	17.2	–
	Bt3	1.30	9.83	88.9	4.81	0.60	0.14	0.66	0.12	0.61	10.5	16.1	–
	Bt4	1.84	10.7	87.5	4.62	0.54	0.11	1.38	0.14	0.52	10.5	22.5	–
	C	15.3	54.7	29.9	4.62	0.25	0.18	0.94	0.30	0.14	11.4	14.9	–
190	A	11.4	34.0	54.6	6.01	7.80	0.81	1.01	4.52	1.25	22.1	34.5	–
	2Bt1	0.12	21.7	78.2	4.75	1.32	0.26	0.75	0.63	0.75	12.7	19.0	–
	2Bt2	0.15	14.5	85.4	4.65	1.05	0.21	0.72	0.22	0.60	14.3	12.0	–
	2Bt3	0.15	13.4	86.4	4.56	0.80	0.16	0.79	0.16	0.59	13.4	13.0	–
240	A	0.95	20.8	78.3	4.78	7.40	0.54	0.84	1.37	1.88	14.9	31.0	–
	Bt1/Bo	4.50	26.3	69.2	4.62	1.25	0.19	1.39	0.07	0.38	13.0	18.0	–
	Bt2/Bo	11.3	33.4	55.4	4.71	0.86	0.05	1.15	0.05	0.44	13.7	14.3	–
	BC	13.3	36.9	49.7	4.62	0.53	0.21	1.50	0.31	0.63	12.7	25.9	–

[a]Soil organic carbon.
[b]Cation exchange capacity of fine earth
[c]Base saturation percentage for fine earth.
[d]++, strong reaction; +, weak reaction; –, no reaction.

retarded in the topsoil of the forest profiles (240 and 190) by active biotic recycling and consequently a reduction in net leaching.

Aluminosilicate clay minerals

Figure 4 and Table 5 show that the main XRD peaks throughout were for kaolinite and illite. Chlorite, vermiculite, vermiculite–illite interstratified minerals, quartz and gibbsite were variable and their peaks were possibly affected by the presence of Fe sesquioxides. The interstratified vermiculite–illite (V–I) minerals in the profiles on the lower benches might be transitional stages in the desilication of 2:1 to 1:1 phyllosilicates (Herbillon *et al.*, 1981; Rice *et al.*, 1985; Ryan & Huertas, 2009). In general, the XRD and chemical results divide the soil samples into two sets; profiles 240–100 contain less illite but more kaolinite and sesquioxides, and profiles 90–15 have more illite, interlayered minerals and quartz, and less kaolinite and gibbsite.

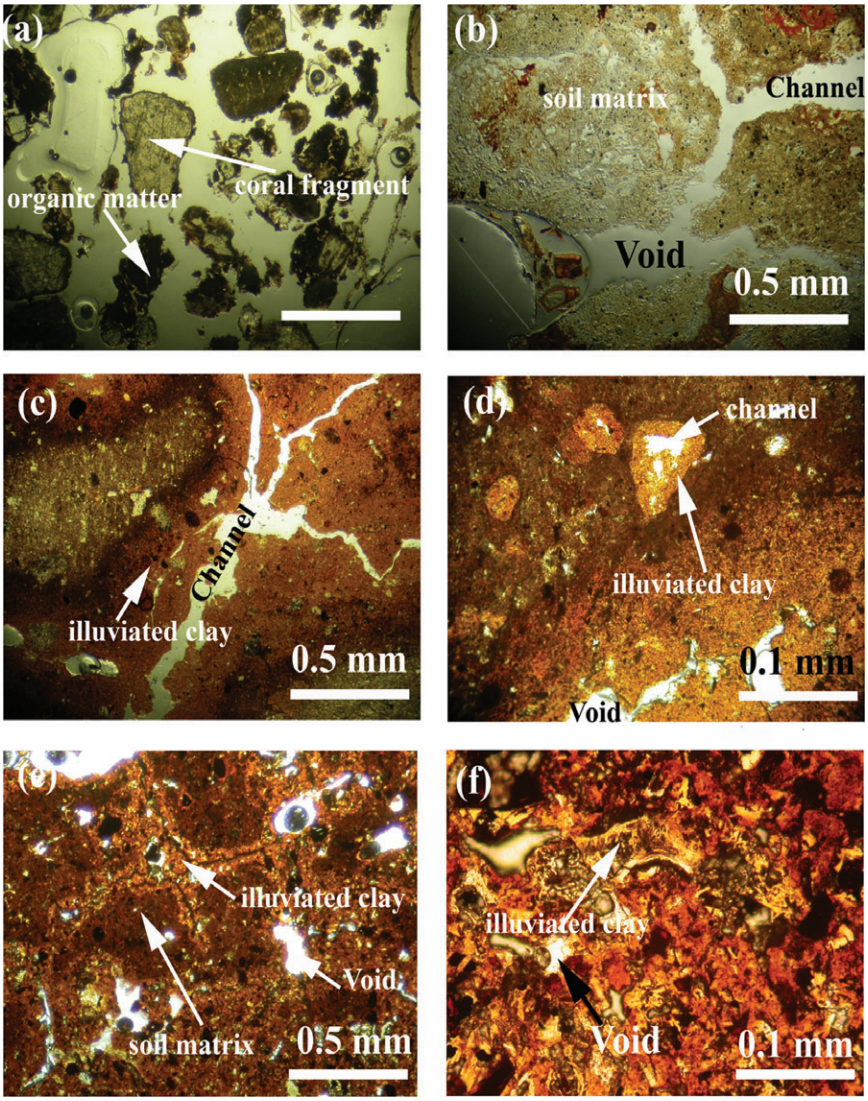

Figure 2 Plane polarized light images of thin sections of subsoil horizons: (a) profile 15, C, (b) profile 20, Bw, (c) and (d) profile 100, Bt1, (e) and (f) profile 240, Bt1.

Principal component analysis

The first two principal components (Figure 5) account for 63.0% of the total variance (Table 7). The first, PC1, accounts for 44.2% of this, and relates to overall weathering, leaching and desilication. Clay, the Al and Fe sesquioxides and TiO_2 have large positive eigenvector values, whereas pH, exchangeable Ca, BS, total Ca and Mg have large negative values (Figure 5a and Tables S1 and S2). The second component, PC2, accounts for 18.8% of the total variance and appears to relate to aeolian deposition of micaceous loess because exchangeable K and silt have positive eigenvector values (Figure 5a and Tables S1 and S2). The plot of the profile scores in the plane of components 1 and 2 (Figure 5b) supports these interpretations. Profile 15 is clearly differentiated from the others on PC1 because of the presence of coral. The PC scores above the lowest bench generally decrease with elevation. The trend with elevation is more evident above 100 m, where coral is negligible, but it is somewhat obscured in the intermediate profiles 20, 50 and 90 by lithological heterogeneity and possibly also by anthropogenic disturbance.

Weathering indices

The indices for CIA and relative base loss rapidly reached constant levels (Figure 6a,b) and did not differentiate between the soil on the intermediate and upper benches. However, SiO_2/Al_2O_3 and $SiO_2/(Fe_2O_3+Al_2O_3)$ were strongly correlated with elevation ($r = 0.775$, $P < 0.05$) (Figure 6c,d), which indicates that desilication and the accumulation of free Al and Fe continue throughout the weathering sequence.

Discussion

Methodological and data limitations

A potential methodological limitation in the interpretation of our results as a chronosequence is the assumption that regolith and soil

Table 4 Total, dithionite-citrate-bicarbonate and oxalate-extractable Fe and Al

Profile	Horizon	Fe_t / g kg^{-1}	Al_t	Fe_d	Al_d	Fe_o	Al_o	Fe_d/Fe_t	Fe_o/Fe_d	$(Fe_d - Fe_o)/Fe_t$
15	A	15.8	25.3	3.69	1.81	1.43	2.89	0.23	0.39	0.14
	C1	12.3	20.3	3.24	1.85	1.19	2.64	0.26	0.37	0.17
	C2	11.3	19.9	2.77	1.74	1.06	2.31	0.25	0.38	0.15
	C3	6.48	12.4	1.15	1.18	0.67	1.12	0.18	0.58	0.07
20	A	29.0	90.0	6.90	10.3	3.49	16.5	0.24	0.51	0.12
	Bw	23.0	71.0	5.80	6.72	3.15	2.49	0.26	0.54	0.12
	BC	ND	5.7	5.82	2.69	5.42	2.99	ND	0.93	ND
	C	30.0	71.0	3.68	1.66	5.06	1.91	0.12	1.38	ND
50	A	74.9	80.3	42.2	10.6	6.05	5.06	0.56	0.14	0.48
	Bt	73.8	88.2	46.8	10.8	6.97	6.00	0.63	0.15	0.54
	2A	69.7	68.7	47.1	11.8	13.6	6.89	0.68	0.29	0.48
	2Bt	81.0	81.7	58.3	14.2	5.98	6.50	0.72	0.10	0.65
	2C	67.0	108.0	36.0	9.53	8.27	8.43	0.54	0.23	0.41
90	A	64.5	53.4	22.0	4.39	4.72	4.11	0.34	0.21	0.27
	AB	63.5	63.4	49.5	10.3	5.72	4.96	0.78	0.12	0.69
	Bt1	77.8	84.0	51.0	9.79	4.68	4.68	0.66	0.09	0.60
	Bt2	69.6	63.8	46.4	8.83	5.18	4.58	0.67	0.11	0.59
	BC	78.4	84.5	33.9	6.90	4.92	4.87	0.43	0.15	0.37
100	A	59.3	84.3	35.2	7.65	4.34	3.31	0.59	0.12	0.52
	AB	53.7	74.0	38.1	7.91	4.75	3.36	0.71	0.12	0.62
	Bt1	62.0	81.7	46.2	9.23	2.68	3.33	0.75	0.06	0.70
	Bt2	59.6	64.2	48.2	10.9	2.54	4.38	0.81	0.05	0.77
	BC	44.8	71.5	23.7	6.47	1.38	3.54	0.53	0.06	0.50
170	O/A	68.1	*ND*	41.7	12.9	2.62	3.60	0.61	0.06	0.57
	Bt1	76.5	89.8	48.7	10.5	1.62	3.28	0.64	0.03	0.62
	Bt2	75.5	93.0	46.7	11.4	1.40	3.50	0.62	0.03	0.60
	Bt3	75.8	90.5	44.8	12.1	1.35	3.56	0.59	0.03	0.57
	Bt4	73.5	97.8	43.1	10.7	1.62	3.85	0.59	0.04	0.56
	C	58.6	101.0	23.1	5.66	1.85	3.42	0.39	0.08	0.39
190	A	ND	51.3	44.1	15.2	9.72	9.14	ND	0.22	ND
	2Bt1	68.6	78.0	61.3	13.1	9.51	4.97	0.89	0.16	0.75
	2Bt2	71.5	77.7	69.8	14.0	5.61	4.22	0.98	0.08	0.90
	2Bt3	78.3	96.3	60.3	18.7	5.19	4.37	0.77	0.09	0.70
240	A	93.9	60.8	82.2	20.2	6.53	4.40	0.88	0.08	0.81
	Bt1	94.8	97.2	54.9	11.5	4.93	4.79	0.58	0.09	0.53
	Bt2	77.2	71.6	57.4	12.1	3.20	4.65	0.74	0.06	0.70
	BC	98.9	89.5	55.9	11.3	2.71	4.44	0.57	0.05	0.54

t = X-ray fluorescence totals, d = dithionite-citrate-bicarbonate, o = oxalate, ND = not determined.

age increase with terrace elevation. This is not always valid (Dorji *et al.*, 2009), but it does appear to hold for Green Island (Chen & Liu, 1992).

Another complication is climatic and physiographic variation during the late Quaternary and within the time-scales of the older soils. The elevation of the surfaces is attributed mainly to tectonic uplifts, but fluctuations in sea level during the late Quaternary that exposed the coral formations on the lower terraces also affected the island's erosional base levels. Furthermore, there were periods in the late Pleistocene and early Holocene in which the climate of Green Island was cooler and probably drier than at present, and periods in the mid- and late-Holocene that were warmer and more humid (Liew & Hsieh, 2000; Morimoto *et al.*, 2007).

There are minor lithological heterogeneities because of the coral in the younger soils and some subordinate basaltic bodies in the predominantly andesitic rocks. Basalt weathers rapidly in the humid tropics and tends to result in soil with larger clay and iron sesquioxide contents and more eutric base status than less mafic rocks. Basalt-derived soil tends towards the Nitisols in the WRB classification. The blocky primary structure and weak micro-pedality in profile 240 appear somewhat nitic. Its main chemical and mineralogical attributes do not indicate obvious basaltic lithological discontinuities, but the Ti/Zr ratios are larger in this profile than in those on the lower benches (Table 8), which suggests that its parent material might be more basaltic (Petersen, 1983).

Another potential source of lithological heterogeneity is aeolian material. Aeolian imports have been noted in soil throughout the western Pacific, including the main island of Taiwan (Cheng *et al.*, 2011), Kyushu (Miyamoto *et al.*, 2010), New Caledonia, Guam and as far afield as Hawaii Dymond *et al.*, 1974). All the soil

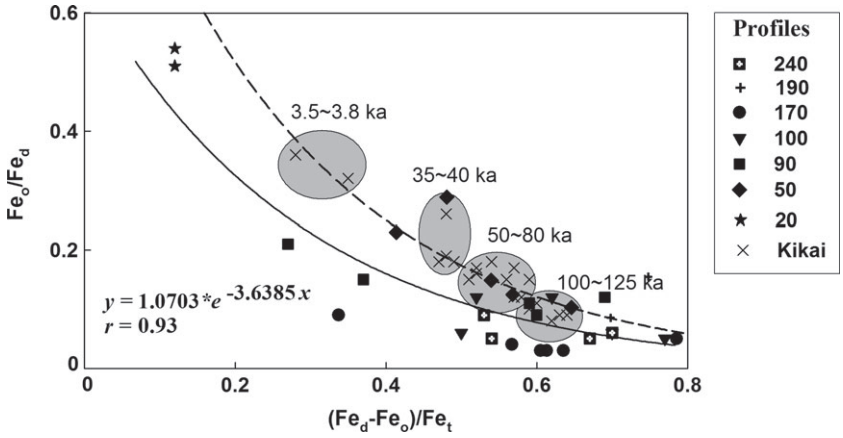

Figure 3 Indices of activity plotted against crystallinity for free iron sesquioxides in Green Island for profiles 20–240. Plots clustered by age for Kikai Island (Ryukus) after Maejima *et al.* (2000) for comparison. In the equation, x represents $(Fe_d - Fe_o)/Fe_t$, and y is Fe_o/Fe_d. The dashed line relates to the soil on KiKai Island, Japan (Maejima *et al.*, 2000), and the solid line represents the soil on Green Island, Taiwan.

Table 5 Aluminosilicate clay minerals

Profile	Horizon	Depth / cm	V	V–I	HIV	C	M	K	G	Q
20	A	0–10	+	+	+	–	+++	+++	+	++
	Bw	10–25	+	+	+	–	+++	+	++	++
	BC	25–70	+	+	+	–	+++	+++	–	++
	C	> 70	+	+	+	–	++	+++	–	++
50	A	0–25	+	+	–	–	++	+++	+	++
	Bt	25–50	+	+	–	–	++	+++	+	++
	2A	50–75	+	+	–	–	++	+++	–	+++
	2Bt	75–100	+	+	–	–	+++	+++	–	++
	2C	> 200	+	+	–	–	++	+++	–	+
90	A	0–10	+	+	–	–	+++	+++	+	++
	AB	10–25	+	+	+	–	++	+++	+	++
	Bt1	25–48	+	+	+	–	++	+++	+	++
	Bt2	48–75	+	+	–	–	++	+++	+	++
	BC	75–110	+	+	–	–	+	+++	–	+
100	A	0–18	+	+	+	+	++	+++	++	+++
	AB	18–35	+	+	+	+	+	++++	+	++
	Bt1	35–67	+	+	–	–	++	+++	+	+++
	Bt2	67–92	+	+	+	–	+	+++	+	++
	BC	92–120	+	+	+	–	+	+++	+	++
170	O/A	0–24	+	+	+	–	++	+++	+	–
	Bt1	24–50	+	+	–	–	++	++++	+	+++
	Bt2	50–70	+	+	–	–	++	++++	+	++
	Bt3	70–100	+	+	+	–	++	++++	+	++
	Bt4	100–140	+	+	+	–	++	++++	+	+
	C	> 200	+	+	–	–	+		+	++
190	A	0–20	+	+	+	–	+	+++	+++	++
	2Bt1	20–45	+	+	+	–	+++	+++	+	++
	2Bt2	45–70	+	+	+	–	+++	+++	+	++
	2Bt3	70–100	+	+	+	–	++	++++	+	++
240	A	0–15	+	+	–	+	++	++++	+	++
	Bt1	15–40	+	–	–	–	+	++++	+	+
	Bt2	40–60	+	+	–	–	+	++++	+	++
	BC	60–90	+	+	+	–	++	++++	+	+

V, vermiculite; V–I, vermiculite–illite interstratified minerals; M, mica; HIV, hydroxy interlayer vermiculite; K, kaolinite; Q, quartz; G, gibbsite; C, chlorite. Semi-quantitative visual assessments of peak strength: –, none; +, weak; ++, moderate; +++, strong; ++++, prominent.

Table 6 Gains and losses of total elements and clay

Profile	Horizon	Thickness / cm	Strain / %	Fe	Al	Si	K	Ca	Mg	Clay
20	A	0–10	0.18	−21	5.0	−18	7.0	−17	−23	−14
	Bw	10–25	0.14	−29	−7.0	−13	3.0	−58	−68	23
	BC	25–70	−0.31	−83	−95	−17	−55	−61	−86	−19
	C	> 70	0	0	0	0	0	0	0	0
	Mean[a]		−14.3	−62	−62	−16	−33	−54	−73	−8.9
90	A	0–10	0.18	−13	−33	−11	35	35	20	20
	AB	10–25	−0.06	−29	−34	−15	51	33	−19	11
	Bt1	25–48	−0.22	−26	−26	−4.0	54	−4.0	0	−6.0
	Bt2	48–75	−0.10	−22	−34	−20	−3.0	−3.0	−13	10
	BC	75–110	0	0	0	0	0	0	0	0
	Mean[a]		−9.05	−23	−31	−13	30	9.1	−5.8	6.6
100	A	0–18	−0.46	−35	−42	−50	−10	−15	−36	−18
	AB	18–35	−0.47	−41	−49	−54	−4.0	185	−46	−8.0
	Bt1	35–67	−0.59	−53	−53	−58	67	−52	−38	−24
	Bt2	67–92	−0.28	−5.0	−36	−57	22	−16	−5.0	27
	BC	92–120	0	0	0	0	0	0	0	0
	Mean[a]		−46	−34	−46	−56	26	8.6	−30	−5.9
240	A	0–15	0.16	30	−29	−18	119	787	16	36
	Bt1	15–40	−0.12	50	15	−30	41	−26	−45	20
	Bt2	40–60	0.16	13	12	−1.0	59	9.0	48	28
	BC	60–90	0	0	0	0	0	0	0	0
	Mean[a]		4.48	6.2	10	−18	66	189	1.0	27

[a]Weighted for horizon thickness: mean = 100* (value * horizon depth/total depth).

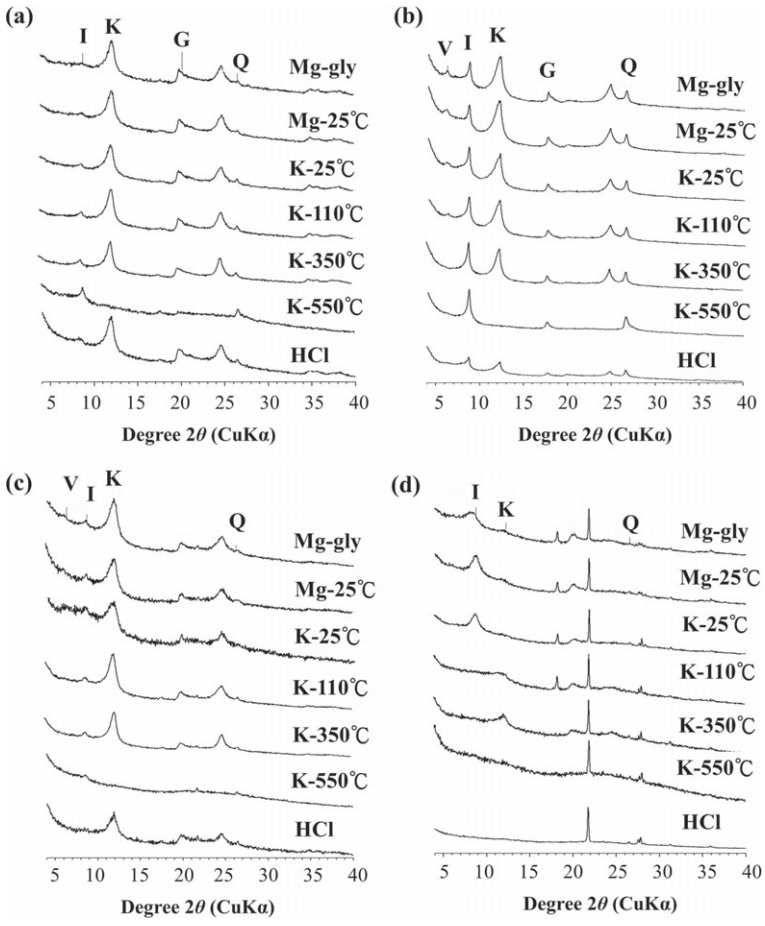

Figure 4 The X-ray diffractometer (XRD) diffractograms of: (a) Bt2 in Profile 240, (b) Bt3 in profile 190, (c) Bt2 in profile 50 and (d) Bw in profile 20.

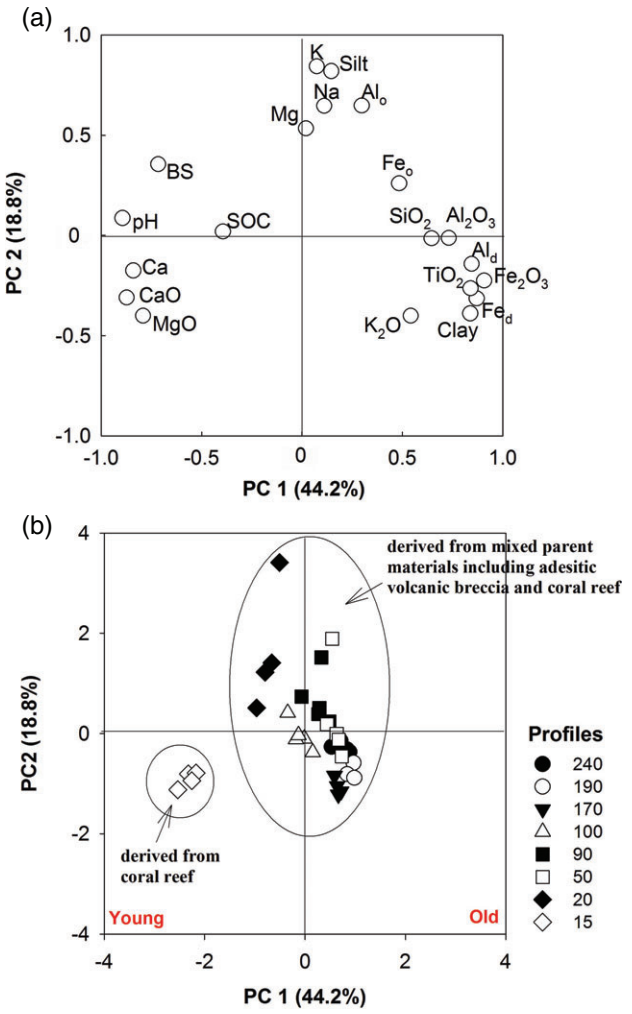

Figure 5 Principal component (PC) analysis: (a) eigenvector values of variables plotted in the plane of principal components 1 and 2 and (b) PC scores for individual horizons of profiles plotted in the plane of PC1 and 2. The shape of the symbol indicates the profile number.

of Green Island is likely to contain windblown material, but the quantity is likely to increase with surface age and elevation. The main sources are micaceous loess from northeastern Asia and tephra from recently active volcanoes in Kyushu and the Ryukyus (Eden *et al.,* 1996). The SiO_2/Al_2O_3 values of the soil in profiles 15 and 20 ranged from 4.4 to 5.2, similar to those of loess in China (Cheng *et al.*, 2011). The silt, K and Mg eigenvector values on PC2 also suggest a micaceous source. The marked increase in silt contents from profile 190 to profile 240 is unusual because silt usually weathers and decreases during ferralization. Although the silt appears to be mostly aeolian, there might also be some pseudo-silt formed by the ferralic aggregation of clay particles (Figure 2f).

Ferralization

Changes with elevation that suggest that the soil of the Green Island benches forms a ferralic-trending chronosequence include: increase in clay content, decrease in textural differentiation, increase in rubefaction, decrease in stone content, increased profile depth, decrease in pH, decreases in exchangeable cation contents and BS in soil, disappearance of coral, decrease in primary minerals in the thin sections, increase in kaolinite and decrease in illite in the

Table 7 The eigenvalues and percentage variance explained from a principal component analysis

Order	Eigenvalue	Percentage variance	Accumulated percentage variance
1	9.28	44.2	44.2
2	3.95	18.8	63.0
3	2.24	10.7	73.7
4	1.21	5.75	79.4

Table 8 The Ti/Zr ratios

Profile	Horizon	Ti / mg kg^{-1}	Zr / mg kg^{-1}	Ti /Zr	Profile mean Ti/Zr
20	A	2.57	0.22	11.5	13
	Bw	3.60	0.23	15.9	
	BC	3.24	0.22	14.8	
	C	2.98	0.27	11.2	
50	A	6.81	0.17	39.0	28
	Bt	6.52	0.22	29.7	
	2A	7.01	0.25	28.2	
	2Bt	4.96	0.21	24.1	
	2C	4.58	0.22	21.3	
90	A	5.00	0.23	21.9	21
	AB	4.95	0.25	20.0	
	Bt1	6.03	0.24	24.8	
	Bt2	3.44	0.14	25.0	
	BC	2.45	0.22	11.0	
100	A	4.27	0.21	20.3	30
	AB	5.18	0.18	28.8	
	Bt1	6.06	0.17	35.5	
	Bt2	5.14	0.15	34.5	
	BC	4.53	0.14	32.2	
170	O/A				
	Bt1	6.16	0.24	25.9	24
	Bt2	6.01	0.26	23.0	
	Bt3	5.08	0.19	27.2	
	Bt4	4.82	0.21	22.8	
	C	5.10	0.22	23.1	
190	A	6.78	0.24	28.3	31
	2Bt1	7.88	0.26	30.2	
	2Bt2	7.03	0.19	36.9	
	2Bt3	6.03	0.20	30.6	
240	A	9.35	0.18	52.7	60
	Bt1	9.31	0.16	59.6	
	Bt2	7.02	0.12	58.3	
	BC1	9.38	0.14	64.8	
	BC2	8.05	0.13	63.1	

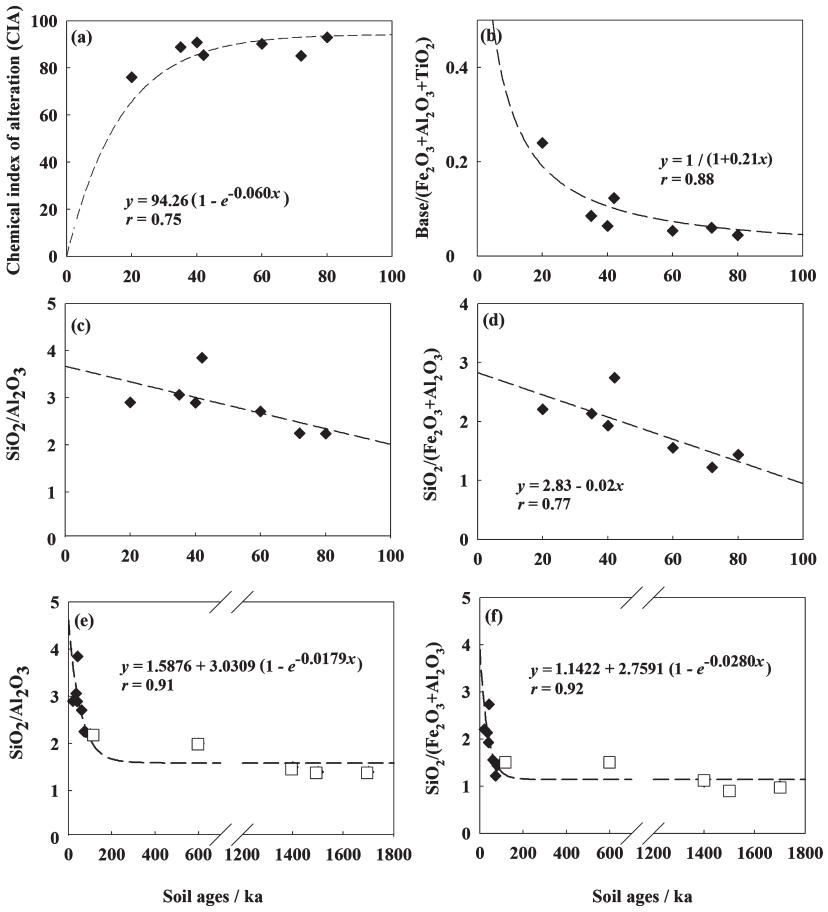

Figure 6 Weathering indices plotted against estimated soil age of Green Island profiles: (a) chemical index of alteration, $CIA = Al_2O_3/(Al_2O_3 + CaO + Na_2O + K_2O) \times 100$, (b) base depletion = $(CaO + Na_2O + K_2O + MgO)/(Fe_2O_3 + Al_2O_3 + TiO_2)$, (c and e) SiO_2/Al_2O_3, (d and f) $SiO_2/(Fe_2O_3 + Al_2O_3)$; time-scales in (e) and (f) are extended by combination with the data (open squares) of Zhang *et al.* (2007). The equation in each subfigure gives the prediction for relative soil ages by the given index.

clay minerals and increase in the Fe, weathering and strain indices. These features indicate that soil development on Green Island is dominated by sustained leaching, desilication and the accumulation of ferric sesquioxides, with a peak of increasing and then declining argilluviation.

Some features, however, such as the moderate blocky structure and absence of micropedality in the subsoil of the higher profiles do not accord with this simple model. Furthermore, the overall trend towards desilication is interrupted mineralogically by the appearance of interlayered vermiculitic and chloritic aluminosilicates in the soil on the intermediate benches. These minerals contribute to the development of pronounced blocky subsoil structures in these soils. Another apparent anomaly is that the Al_t, Al_d and Al_o varied erratically above the 15-m terrace, and free Al sesquioxides did not increase systematically in content and crystallinity with altitude and soil age. Gibbsite contents were generally small and showed no clear altitudinal trends; the larger values were in the topsoil of profiles 100 and 190. The larger peak for vermiculite in the topsoil of profile 190 was matched by a large value for Al_o, but not for the other Al extracts. One possible interpretation of this pattern is that initially weathered Al is resilicated into the secondary aluminosilicates (Sak *et al.*, 2004). The weak altitudinal trend in Al explains why the SiO_2 / Al_2O_3 desilication index correlates less well with altitude than does $SiO_2/(Fe_2O_3 + Al_2O_3)$ (Figure 6c,d). The SiO_2/Al_2O_3 ratio correlates with age in the basaltic soil on Hainan, but that is over a longer time than is spanned by the Green Island sequence (Zhang *et al.*, 2007). It is possible that free Al and gibbsite might accumulate later as ferralization intensifies and secondary kanditic aluminosilicates are eventually weathered (Kleber *et al.*, 2007).

The trends in mineralogy and strain in the Green Island soil are similar to those in soil on marine terraces on the eastern coast of mainland Taiwan (Tsai *et al.,* 2007) and also on bevelled surfaces on Kikai Island in the Ryukyu archipelago, about 1100 km to the northeast (Nagatsuka, 1972; Maejima *et al.*, 2000).

The rubefaction, the large contents and crystallinity of the Fe sequioxides make Profile 240 (Table 9) appear to be an incipient Ferralsol in WRB (Hapludox in Soil Taxonomy). The clay skins and angular blocky structure (Isbell, 1994) and the CEC:clay ratios, however, are borderline for ferralic (oxic) horizons (Table 9). The textural B horizons in the profiles at intermediate elevations appear to be argillic, and profiles 190 and 170 qualify as Cutanic Acrisols (Hapludult). The less intense leaching and larger BS of profiles 100 to 50 mean that they are Lixisols (Udalfs), although some clay ratios are small. Profile 20 is a Cambisol (Eutrudept) and profile 15 is a rudimentary Haplic Arenosol (Udipsamment) (Table 9). The free carbonates and high base status in profile 100 (Table 3) indicate

Table 9 Pedotaxonomic criteria and soil classification

	Clay ratio	Clay skins		Bt	B	Soil classification	
Profile	Bt / A	Profile description	Thin section[a]	CEC / clay	% Base saturation	World Reference Base[b]	Soil Taxonomy[c]
15	1.06	0	None	–	100	Haplic Arenosol (Eutric)	Typic Udipsamment
20	1.31	2	Unsorted	–	79	Haplic Cambisol (Eutric)	Typic Eutrudept
50	1.00	2	MD (15%)	12–39	59	Haplic Lixisol – Cambisol (Eutric)	Hapludalf – Eutrudept
90	1.04	3	ML (20%)	8–14	85	Cutanic Lixisol (Hypereutric)	Typic Hapludalf
100	1.20	3	ML (30%)	8–12	98	Cutanic Lixisol (Hypereutric)	Typic Hapludalf
170	1.18	3	ML (30%)	7–10	16	Cutanic Acrisol	Typic Hapludult
190	1.56	3	ML (30%)	10–12	12	Cutanic Acrisol	Typic Paleudult
240	< 1.0	3	NL (50%)	12–19	14	Acric (Alic) Ferralsol	Typic Hapludox

[a]N, non-laminated; M, micro-laminated; L, limpid clay coating; D, dusty clay coating; the percentage in parenthesis is the amount of clay coating in field view under the microscope (25X, PPL).
[b]World Reference Base (IUSS Working Group WRB, 2015).
[c]USDA Soil Taxonomy (Soil Survey Staff, 2014).

that the trend of increased leaching and weathering with elevation is irregular.

Quantification of the rate of ferralization on Green Island requires the terraces to be dated. Using the regional eustatic sea-level curve that is derived from radiometrically dated terraces in New Guinea (Chappell *et al.*, 1996) and southwestern Japan (Maejima *et al.*, 2000), Chen & Liu (1992) estimated the ages of the seven terraces they identified on Green Island as: about 80 ka for the 245–255 m level, 70 ka (190–200 m), 60 ka (165–175 m), 50 ka (140–150 m), 40 ka (80–90 m), 33∼35 ka (20–40 m) and < 5.5 ka, (2–15 m). However, the southwest Pacific is a region of intense and spatially variable tectonic activity, and terraces in different locations have been uplifted spasmodically at different times and rates, which makes the interpolation of chronology from altitude somewhat approximate (Tsai *et al.*, 2006). The carbonates of the two lowest Green Island terraces have been ^{14}C dated at 33–36 ka for the 20-m bench and 1–9 ka for the lowest level, which are close to the interpolated estimates (Chen & Liu, 1992). Overall, the rate of tectonic uplift of Green Island during the late Quaternary is estimated at 2–4 mm year^{-1}.

The transition from argilluvial to ferralitic pedogenesis therefore appears to be rapid, which is characteristic of parent materials with large contents of ferromagnesian minerals (Zhang *et al.*, 2007). The transition from Andosols to Ferralsols, however, in the classic sequence on basalt flows in Hawaii has been estimated to have taken more than 1.4 Ma (Vitousek, 2004). The combination of free drainage and moderately large Fe contents of the andesitic parent materials on Green Island appears to favour ferralization although the minor coralline limestone constituents might retard acidification.

Conclusions

The progression along the pedogenic path from Arenosols (Entisols) through Cambisols (Inceptisols), argillic Lixisols and Acrisols (Alfisols and Ultisols) to incipient Ferralsols (Oxisols) shown by the soil of Green Island appears to be unusually rapid. This is attributed to the combination of fine textures and free drainage. The ferralic features, however, are still only incipient and there might be more pronounced desaturation, sesquioxide crystallization and segregation, degradation of argillans and the development of compound micro-pedality with further ageing. However, there is much potential for disruption and pedogenic re-setting by tectonic activity and geomorphic disturbance of regoliths in regions along active plate margins such as the southwest Pacific.

Supporting Information

The following supporting information is available in the online version of this article:

Table S1. Pearson's correlation coefficients among variables ($n = 37$).

Table S2. Eigenvectors of variables from a principal component analysis.

Acknowledgements

The authors thank the Ministry of Science and Technology of Taiwan, Republic of China, for financially supporting this research under contract number MOST-103-2313-B-020-007-MY2. The authors are also grateful to Ms Pei-Yi Yu from the Biodiversity Research Center, Academia Sinica, Taipei, Taiwan, for sampling and part of the analyses. We thank the journal's reviewers and Editor-in-Chief for many helpful comments on earlier versions.

References

Baillie, I.C. 1996. Soils of the humid tropics. In: *The Tropical Rain Forest: An Ecological Study*, 2nd edn (ed. P.W. Richards), pp. 256–286. Cambridge University Press, Cambridge.

Beinroth, F.H., Uehara, G. & Ikawa, H. 1974. Geomorphic relationships of Oxisols and Ultisols on Kauai, Hawaii. *Proceedings of Soil Science Society of America*, **38**, 128–131.

Blume, H.P. & Schwertmann, U. 1968. Genetic evaluation of profile distributions of aluminum, iron and manganese oxides. *Soil Science Society of America Journal,*. **33**, 438–444

Brimhall, G.H. & Dietrich, W.E. 1987. Constitutive mass balance relations between chemical composition, volume, density, porosity, and strain in metasomatic hydrochemical systems: results on weathering and pedogenesis. *Geochimica et Cosmochimica Acta*, **51**, 567–587.

Brindley, G.W. & Brown, G. (eds) 1980. *Crystal Structures of Clay Minerals and Their X-ray Diffraction*. *Mineralogical Society Monograph*, Volume **5**. Mineralogical Society, Twickenham.

Chappell, J., Omura, A., Esat, T., McCulloch, M., Pandolfi, J., Ota, Y. *et al.* 1996. Reconciliation of late Quaternary sea levels derived from coral terraces at Huon Peninsula with deep sea oxygen isotope records. *Earth & Planetary Science Letters*, **141**, 227–236.

Chen, Y.G. & Liu, T.K. 1992. Vertical crustal movement of a tectonic uplifting volcanic island – Lutao. *Journal of the Geological Society of China*, **35**, 231–246.

Cheng, C.H., Jien, S.H., Tsai, H. & Hseu, Z.Y. 2011. Geomorphologic and paleoclimatic implications of soil development from siliceous materials on the coral-reef terrace of an off-shore island in southern Taiwan. *Soil Science & Plant Nutrition*, **57**, 114–127.

Dorji, T., Caspari, T., Bäumler, R., Veldkamp, A., Jongmans, A., Tshering, K. *et al.* 2009. Soil development on Late Quaternary river terraces in a high montane valley in Bhutan, Eastern Himalayas. *Catena*, **78**, 48–59.

Dymond, J., Biscaye, P.E. & Rex, R.W. 1974. Eolian origin of mica in Hawaiian soils. *Geological Society of America Bulletin*, **85**, 37–40.

Eden, D.N., Frogatt, P.C., Zeng, H.-H. & Machida, H. 1996. Volcanic glass found in Late Quaternary Chinese loess: a pointer to future studies. *Quaternary International*, **34–36**, 107–111.

Egli, M. & Fitze, P. 2000. Formulation of pedologic mass balance based on immobile elements: a revision. *Soil Science*, **165**, 437–443.

Egli, M., Nater, M., Mirabella, A., Raimond, S., Ploetze, M. & Alioth, L. 2008. Clay minerals, oxyhydroxide formation, element leaching and humus development in volcanic soils. *Geoderma*, **143**, 101–114.

Herbillon, A.J., Frankart, R. & Vielvoye, L. 1981. An occurrence on interstratified kaolinite–smectite minerals in a red–black soil toposequence. *Clay Minerals*, **16**, 195–201.

Ho, C.S. 1988. *An Introduction to the Geology of Taiwan: Explanatory Text of the Geologic Map of Taiwan*, 2nd edn. Central Geologic Survey, Taipei.

Huang, W.S., Tsai, H., Tsai, C.C., Hseu, Z.Y. & Chen, Z.S. 2010. Subtropical soil chronosequence on Holocene marine terraces in Eastern Taiwan. *Soil Science Society of America Journal*, **74**, 1271–1283.

Isbell, R.F. 1994. Krasnozems – a profile. *Australian Journal of Soil Research*, **32**, 915–929.

IUSS Working Group WRB 2015. *World Reference Base for Soil Resources 2014. International Soil Classification System for Naming Soils and Creating Legends for Soil Maps*. World Soil Resources Report No 106, FAO, Rome.

Jenny, H. 1980. *The Soil Resource, Origin and Behaviour*. Springer-Verlag, New York.

Kleber, M., Schwenendenmann, L., Veldkamp, E., Roessner, J. & Jahn, J. 2007. Halloysite versus gibbsite: silicon cycling as a pedogenetic process in two lowland neotropical rain forest soils of La Selva, Costa Rica. *Geoderma*, **138**, 1–11.

Klute, A. (ed.) 1986. *Methods of Soil Analysis: Part 1*. American Society of Agronomy, Soil Science Society of America, Madison, WI.

Legros, J.-P. 2012. *Major Soil Groups of the World: Ecology, Genesis, Properties and Classification*. CRC Press, Boca Raton, FL.

Liew, P.M. & Hsieh, M.L. 2000. Late Holocene (2 ka) sea level, river discharge and climate interrelationships in the Taiwan region. *Journal of Asian Earth Sciences*, **18**, 499–505.

Maejima, Y., Nagatsuka, S. & Higashi, T. 2000. Mineralogical composition of iron oxides in the red- and yellow-coloured soils from southern Japan and Yunnan, China. *Soil Science & Plant Nutrition*, **46**, 571–580.

Miyamoto, M., Hamamoto, R. & Yanagi, T. 2010. Sr and Nd isotope compositions of atmospheric dust at the summit of Mt Se, north Kyushsu, southwestern Japan: a marker of dust provenance and seasonal variability. *Geochimica et Cosmochimica Acta*, **77**, 1471–1484.

Morimoto, M., Kayanne, H., Abe, O. & McCulloch, M.T. 2007. Intensified mid-Holocene monsoon recorded in corals from Kikai Island, subtropical northwestern Pacific. *Quaternary Research*, **67**, 204–214.

Nagatsuka, S. 1972. Studies on genesis and classification of soils in warm-temperate region of Southwest Japan, Part 3. Some features in distribution and mode of existence of free iron and aluminum oxides in the soil profile. *Soil Science & Plant Nutrition*, **18**, 147–154.

Nieuwenhuyse, A. & van Breemen, N. 1997. Quantitative aspects of weathering and neoformation in selected Costa Rican volcanic soils. *Soil Science Society of America Journal*, **61**, 1450–1458.

Petersen, M.D. 1983. The use of the 'immobile' elements Zr and Ti in lithochemical exploration for massive sulphide deposits in the Precambrian Pecos greenstone belt of northern New Mexico. *Journal of Geochemical Exploration*, **19**, 616–617.

Rice, T.J., Buol, S.W. & Weed, S.B. 1985. Soil saprolite profiles derived from mafic rocks in the North Carolina piedmont. I Chemical, morphological, and mineralogical characteristics and transformations. *Soil Science Society of America Journal*, **49**, 171–178.

Ryan, P.C. & Huertas, F.J. 2009. The temporal evolution of pedogenic Fe-smectite to Fe-kaolin via interstratified kaolin-smectite in a most tropical chronosequence. *Geoderma*, **151**, 1–15.

Sak, P.B., Fisher, D.M., Gardner, T.W., Murphy, K. & Brantley, S.L. 2004. Rates of weathering rind formation on Costa Rican basalt. *Geochimica and Cosmochimica Acta.*, **68**, 1453–1472.

Soil Survey Staff 2014. *Keys to Soil Taxonomy*, 12th edn. National Resources Conservation Service, U.S. Department of Agriculture, Washington.

Stoops, G. 2003. *Guidelines for Analysis and Description of Soil and Regolith Thin Sections*. Soil Science Society of America, Inc., Madison, WI.

Tsai, H., Huang, W.S., Hseu, Z.Y. & Chen, Z.S. 2006. A river terrace soil chronosequence of the Pakua tableland in central Taiwan. *Soil Science*, **171**, 167–179.

Tsai, C.C., Tsai, H., Hseu, Z.Y. & Chen, Z.S. 2007. Soil genesis along a chronosequence on marine terrace in eastern Taiwan. *Catena*, **71**, 394–405.

Van Reeuwijk, L.P. 1993. *Procedures for Soil Analysis*. Wageningen, International Soil Reference and Information Centre.

Vitousek, P. 2004. *Nutrient Cycling and Limitation. Hawai'i as a Model System*. Princeton University Press, Princeton, NJ.

Zhang, G.-L., Pan, J.-H., Huang, C.-M. & Gong, Z.-T. 2007. Geochemical features of a soil chronosequence developed on basalt in Hainan Island, China. *Revista Mexicana de Ciencias Geologicas*, **24**, 261–269.

Incipient ferralization and weathering indices along a soil chronosequence in Taiwan

Jien, S. H.

2016-09-09

Jien SH, Baillie I, Huang WS, et al., (2016) Incipient ferralization and weathering indices along a soil chronosequence in Taiwan, European Journal of Soil Science, Volume 67, Issue 5, September 2016 , pp. 583–596

http://dx.doi.org/10.1111/ejss.12363